J Mater Sci (2012) 47:5646–5654
DOI 10.1007/s10853-012-6496-x

SYNTACTIC & COMPOSITE FOAMS

Open cell lead foams: processing, microstructure, and mechanical properties

Umut Savaci · Sinan Yilmaz · Mustafa Güden

Received: 23 December 2011 / Accepted: 11 April 2012 / Published online: 26 April 2012

Abstract Open cell lead foams with the porosities between 48 and 74 % were prepared by means of powder metallurgical and casting routes, using ammonium bicarbonate particles, silica beads, and sodium chloride salt particles as space holder. The resulting foam samples structure closely resembled open cell foam structure: each cell had few interconnections with neighboring cells. Small-sized lead (II) fluoride precipitates were microscopically observed in the interior of cells in the foam samples prepared using silica beads as space holder, resulting from the reaction between silica and hydrofluoric acid in the space holder dissolution step. The compression stress–strain curve of foam samples prepared by powder metallurgical route showed brittle deformation behavior following the initial elastic deformation region, while the foam samples prepared by casting route showed characteristic foam deformation behavior: cell edge crushing on the bent cell walls, and cell wall tearing. The collapse stresses, densification strains, and elastic moduli of the prepared foams were further fitted with scaling relations.

U. Savaci
Department of Materials Science and Engineering, İzmir Institute of Technology, 35430 Urla, İzmir, Turkey

S. Yilmaz
İnci Akü Company, Organize Sanayi Bölgesi, 45030 Manisa, Turkey

M. Güden (✉)
Department of Mechanical Engineering, İzmir Institute of Technology, 35430 Urla, İzmir, Turkey
e-mail: mustafaguden@iyte.edu.tr

Introduction

Environmental pollution has been intensified significantly in recent decades. In parallel with this, the efforts to alleviate the pollution have been raised greatly all over the world. One of the major causes of the environmental pollution is the exhaust emissions of the internal combustion engines, requiring the automotive industry to design and produce environmentally friendly novel hybrid-electrical and/or electrical vehicles. The development of electrical vehicles strongly depends on the capacity of the batteries. On the other side, lead-acid batteries are still the ultimate choice for the vehicles. Despite relatively lower production costs, ease of production and recyclability, the conventional lead-acid batteries suffer from relatively low capacity and power, short period of life cycle and heavy weight. A typical lead-acid car battery is as heavy as 14 kg; lead electrodes constitute about 21 % of total weight [1]. One way of reducing the weight of currently used lead-acid batteries is to replace the heavy lead electrodes with low density and high surface area porous lead electrodes [2–4]. Both, the increase in the electrode surface area and the reduction in the electrode weight, increase the utilization efficiency of the positive active material up to 50 %, which is much higher than the conventional grid electrode [2].

Gyenge et al. [5] prepared lead foams by the deposition of lead alloy onto a highly porous, reticulated vitreous carbon foam substrate. The specific surface area of the electrode was three times higher (14 cm^2/cm^3) than the book-mold grid battery electrode (4.6 cm^2/cm^3) and the discharged current densities increased from 7.2 to 37.1 mA/cm^2. Irretier et al. [3] prepared closed cell lead foams using foaming powder compact process. Lead carbonate was used as a gas releasing blowing agent at 450 °C. Tabaatabai et al. [4] prepared open cell lead foams

by electrodepositing lead alloy onto Cu foam substrates. The battery with foam electrode showed 42 % higher capacity density than conventional battery. Dai et al. [6] prepared 88.1 % porous high specific surface area (57 cm^2/cm^3) lead foam through electrodeposition. The foam structure provided higher mass specific capacities up to 44 %. Belhadj et al. [7] manufactured 67–69 % porous tin–lead alloy foams by the negative replication of irregularly shaped salt space holder particles with the average pore sizes between 1.6 mm and 4 mm. Bertolino et al. [8] successfully applied the replication method with the silica beads to produce Cu–Zn–Al foams.

In this experimental study, both powder metallurgical and casting routes, were investigated using ammonium bicarbonate, silica beads, and salt particles as space holder for the processing of open cell lead foams to be used as electrodes in lead-acid batteries. The present study targets the processing lead foams with both sub-millimeter and millimeter pore sizes, and the porosities below and above 70 %. The ultimate goal of the continuing research program is to produce open cell lead foams with optimized microstructure that can allow high current discharge densities, and optimized mechanical properties that can sustain certain secondary operations including fastening, rolling, bending, and cutting without any brittle deformation/fracture. In the present part, only the compression mechanical properties of the prepared foams in sub-millimeter and millimeter pore sizes were reported, while the discharge current densities will be investigated in future.

Experimental

Materials and foam preparation

The powder metallurgical route of foam preparation method, also known as space holder method [9], started with the mixing of lead powder with 50 vol% ammonium bicarbonate space holder. Green powder compacts with a diameter of 25 mm and a thickness of 11 mm were cold compacted at room temperature inside a stainless steel die under the compaction pressures of 71 and 142 MPa. Green compacts were heat treated at 180 °C (determined by TGA analysis) for 2 h to remove the space holder particles. The heat treatment was performed in a vacuum furnace at 0.986 atmospheres to minimize the oxidation of the lead powders during decomposition. The resulting porous green lead powder compacts were then sintered in a tightly closed horizontal tube furnace under high purity (99.998 %) Ar flux (6 cm^3/min) at temperatures ranging between 261 °C (0.8 T_m) and 300 °C (0.9 T_m) for 2 h. The specifications of raw materials used to prepare lead foam samples are tabulated in Table 1. The particle size of the lead powder was between 20 μm (d_{10}) and 96 μm (d_{90}) with an average particle size of 48 μm (d_{50}). The ammonium bicarbonate powder was sieved between 314 and 500 μm to obtain narrower particle size distribution. The particle size ratio of ammonium bicarbonate powder to lead powder is about six, which is in accord with the previous studies, in which the space holder particle size was at least 3–4 times bigger than the metal powder particle size [10–12]. The SEM pictures of used irregular lead and ammonium bicarbonate powder particles are shown in Fig. 1a and b, respectively.

The composition of lead alloy used to prepare open cell lead foams by casting liquid metal around space holding fillers method [9] is tabulated in Table 2. The alloy composition is the same with the composition of the alloy used in conventional lead electrode production. In the casting route, the liquid metal was infiltrated into a space holding filler under pressure. Upon the solidification of the liquid alloy, the space holder was removed using a liquid agent. Two different space holding fillers were used to prepare lead foams: silica beads with an average particle size of 2.5 mm (Fig. 2a), and salt powder with an average particle size of 440 μm (Fig. 2b).

Before infiltration, the spherical silica beads (Sigma S7500 Type-II silica beads) were sieved to obtain an average particle size of 2.5 mm. The sieved silica beads were heat-treated at 650 °C for 2 h to remove the absorbed water. The foam preparation process shown in Fig. 3 was composed of alloy melting and infiltration, and space holder dissolution steps. The process started with the insertion of silica beads into a steel mold. The steel mold accommodating silica beads were heated up to 450 °C inside a furnace, and then solid lead was added into the mold. Infiltration was performed after the complete melting of lead alloy. After solidification of lead alloy, the space holder silica beads were dissolved inside a 75 % hydrofluoric acid (HF) solution for 2 h. The reaction between silica beads and HF is [13]

$$SiO_2 + 4HF \rightarrow SiF_4 + 2H_2O$$

After the completely removal of the silica beads, the foam samples were cleaned with water. The steel mold used for the infiltration process, shown in Fig. 4, consisted

Table 1 The material specifications of lead powder and space holder

Powder	Company	Particle size	Purity (%)
Lead powder	Alfa Aesar	−200 mesh (d_{50}: 48 μm)	99
Ammonium bicarbonate	Merck	−500, +314 μm	98

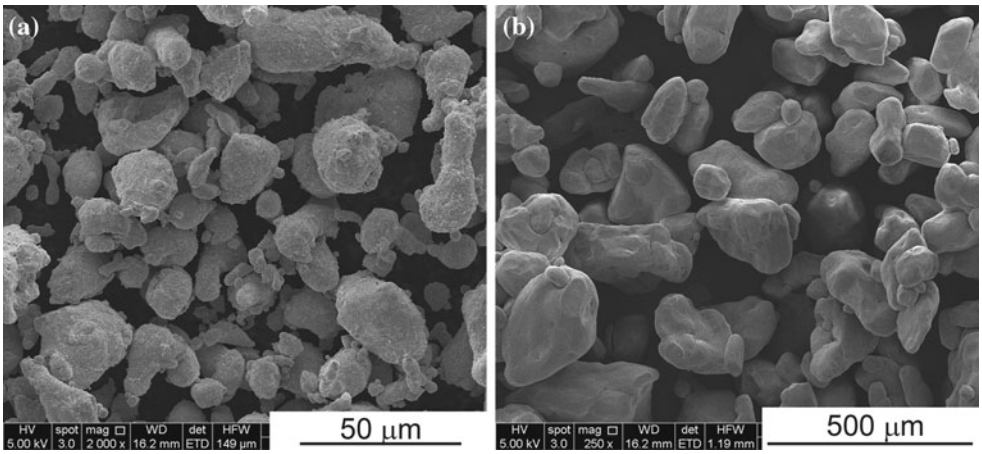

Fig. 1 SEM image of the as-received **a** lead powder, and **b** ammonium bicarbonate particles

Table 2 The composition of lead alloy used in casting

Element	Pb	Ca	Sn	Al	Ag	As	Bi	Cu	Fe	Ni	Te	Zn	Sb	Cd
Weight %	64.85	7.5	25	0.8	0.2	0.1	1	0.1	0.1	0.05	0.05	0.1	0.1	0.05

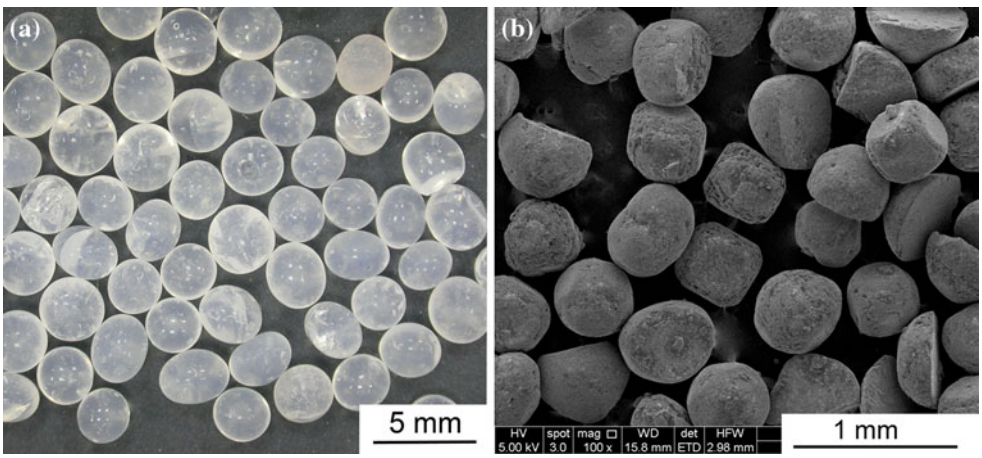

Fig. 2 **a** Optical microscope picture of silica beads and **b** SEM picture of salt particles

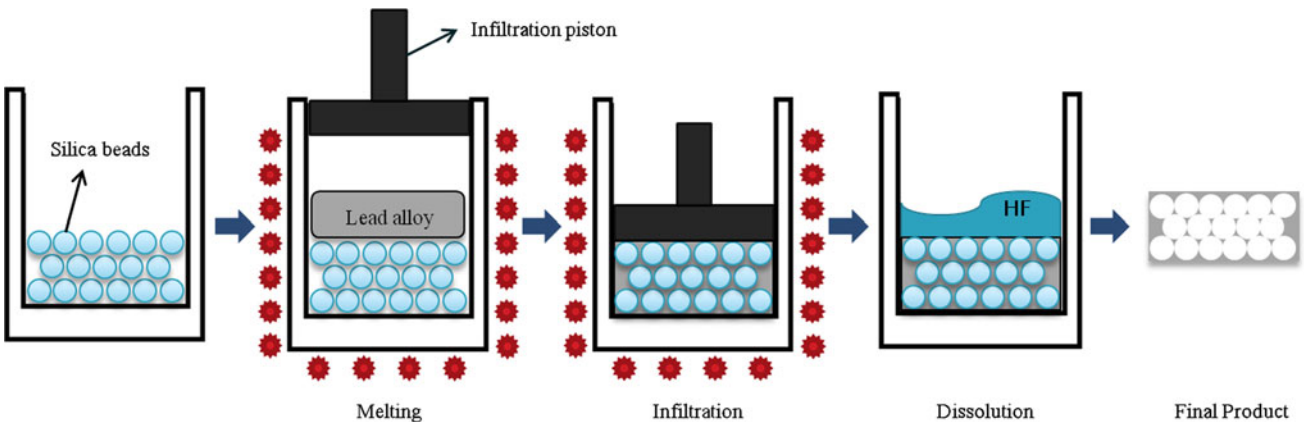

Fig. 3 Schematic of the casting liquid metal around space holding fillers method

of two mating parts mounted with bolts. The mating parts of the mold were demounted after the solidification of lead alloy to remove the infiltrated sample. A piston was used to press the liquid lead alloy into the space holder filler.

The sodium chloride salt powder particle size varies between 500 and 400 μm with an average particle size of 440 μm. The particles had rounded edges and corners (Fig. 2b), providing a denser packing than cubical particles. Before infiltration process salt particles were heat-treated at 90 °C for 10 h in a vacuum furnace to remove any residual water on the particles. The applied infiltration process was the same with the silica beads; the salt particles were inserted into the infiltration mold, and the mold was heated up to 450 °C; then, the liquid lead was infiltrated using the piston. After solidification, salt particles were dissolved in boiling deionized water under vacuum for 2 h, and the process was repeated for several times. The solubility of sodium chloride in water is as high as 39.1 g/100 ml at 100 °C [14]. The applied vacuum allowed water penetration through narrow interconnection regions between pores and provided complete dissolution of salt particles.

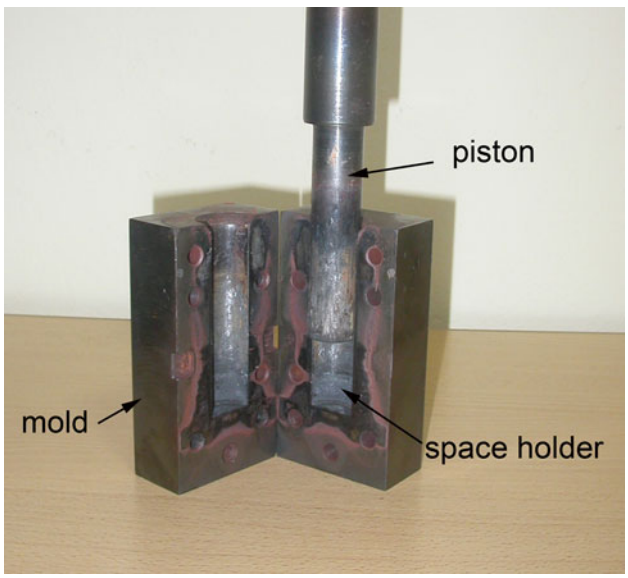

Fig. 4 The picture of the mold used in the infiltration

Characterization

Quasi-static compression tests were conducted on the cylindrical samples; the test samples prepared by powder metallurgical route were 8 mm in diameter and 11 mm in height, and the test samples prepared by casting route were 25 mm in diameter and 20 mm in height. Both types of test samples were prepared by core drilling of the foam samples through the normal to the thickness (parallel to infiltration direction). Quasi-static compression tests were performed using a SCHIMADZU AG-IX universal tension–compression test machine at a strain rate of 1×10^{-3} s^{-1}, following DIN 50134 (ISO 13314) standard testing of metallic materials-compression test of metallic cellular material [12]. At least three compression tests were performed for each foam sample prepared. It was previously shown that the number of cells should be more than 8 across the cross-section area of the test sample in the compression test direction to obtain sample size independent mechanical properties [15]. The number of cells in the tested foam samples was more than the minimum required number of cells. The relative density was determined by measuring weight, and dimensions of foam samples prepared. The volume fraction of the pores (V_f) was calculated using the following relation;

$$V_f = 1 - \frac{\rho_f}{\rho_b} \quad (1)$$

where, $\rho_f$and $\rho_b$are the densities of lead foam and lead alloy, respectively. Microscopic analyses of the foam samples were performed using a Philips XL30-SFEG SEM with an energy dispersive X-ray (EDX) analyzer. Chemical

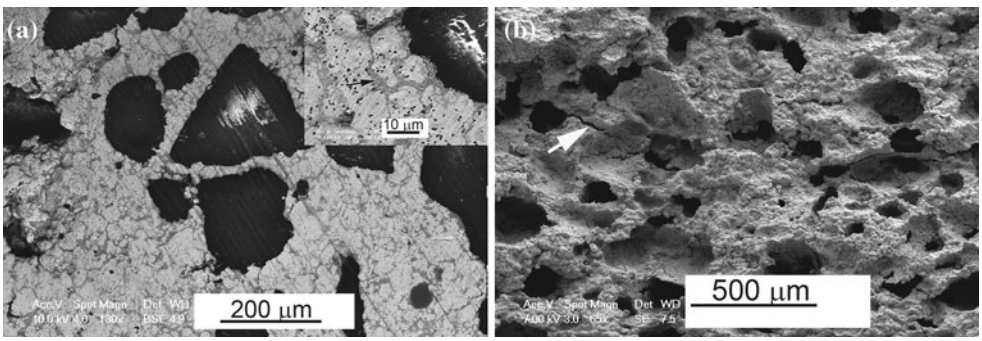

Fig. 5 **a** Microstructure of the polished surface of a foam sample showing pores and oxide layer around particles, and **b** the fracture surface of the tested foam sample

analysis of the lead was performed using a METEC-Spectro IQ-II X-XRF analyzer.

Results and discussion

Foams prepared by powder metallurgical route

The foams prepared at different compaction pressures and sintering temperatures had porosities ranging between 48 and 51 %. The picture of the polished surface of a foam sample prepared by powder metallurgical route is shown in Fig. 5a. In the same micrograph, the grayish regions around particles marked with an arrow in the inset of the figure are found rich in lead and oxygen determined from EDX analysis. These regions contain lead oxide, preventing the sintering lead particles. The SEM image of the typical fracture surface of lead foam prepared by powder metallurgical route is further shown in Fig. 5b. The cracks around the particles (intergranular) indicate the brittle nature of the foams. The compressive stress–strain curves of the foams prepared at different compaction pressures and sintering temperatures are further shown in Fig. 6. As is seen in Fig. 6, the foam samples show brittle deformation behavior following the linear elastic region: the stress values decrease after the collapse stress/initial maximum stress. The samples catastrophically fractured after the maximum stress and showed significant variations in strength values. The maximum stress ranges between 2.6 and 8.9 MPa depending on the processing parameters. The brittle behavior of the foam samples is also in accord with the microscopic observations. The presence of oxide layers on the surfaces of the particles and the oxide formation during heat treatment and sintering cause the brittle deformation of the foams in compression.

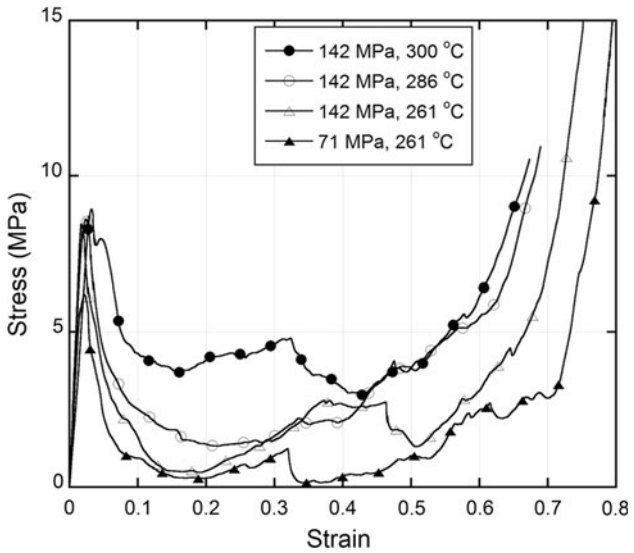

Fig. 6 Compressive stress–strain curve of foam samples prepared by powder metallurgical route at various compaction pressures and sintering temperatures

Foams prepared by casting route

The picture of lead foam after silica beads removal and the cross-section view of a 60 % porous foam are shown in Fig. 7a, b, respectively. As seen in Fig. 7a, b, each cell has interconnections with neighboring cells, confirming an open cell structure of the prepared foam samples. The interconnection points on a cell wall are shown in Fig. 8a. Microscopic analysis showed that each cell had six interconnections on the average, and the interconnections provided the interlinking between the cells after the space holder removal process. Small size precipitates are

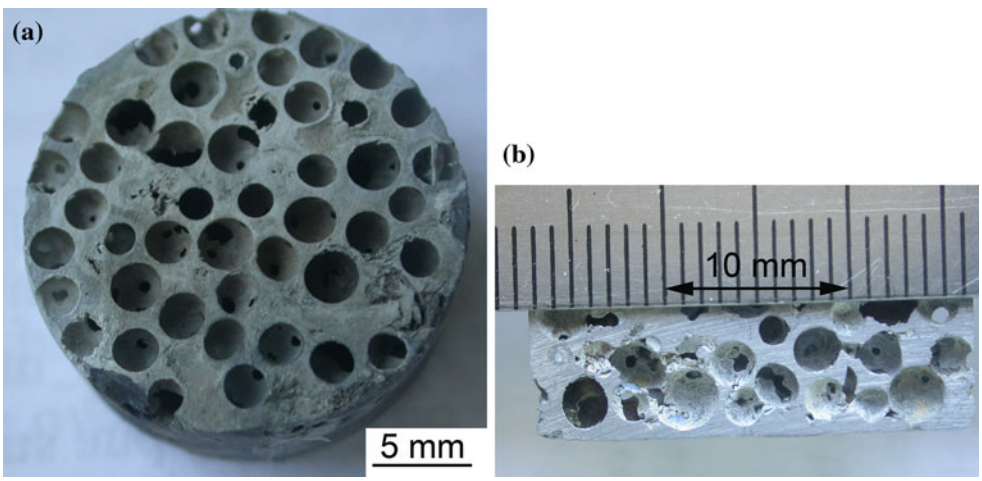

Fig. 7 **a** The picture of a 60 % porous lead foam sample after removing silica beads, and **b** cross-section view, showing the cells and interconnections with neighboring cells

observed on the foam samples surfaces and interior of the cells (Fig. 8b). These are lead (II) fluoride precipitates determined by EDX analysis. It was previously shown that lead (II) fluoride layer covering the surface of lead electrode did not cause passivation of the electrode during charge and discharge [16]. The solubility of lead (II) fluoride in water was reported 0.66 g/l (2.7 mMol/l) [14]; therefore, this layer can also be dissolved in water.

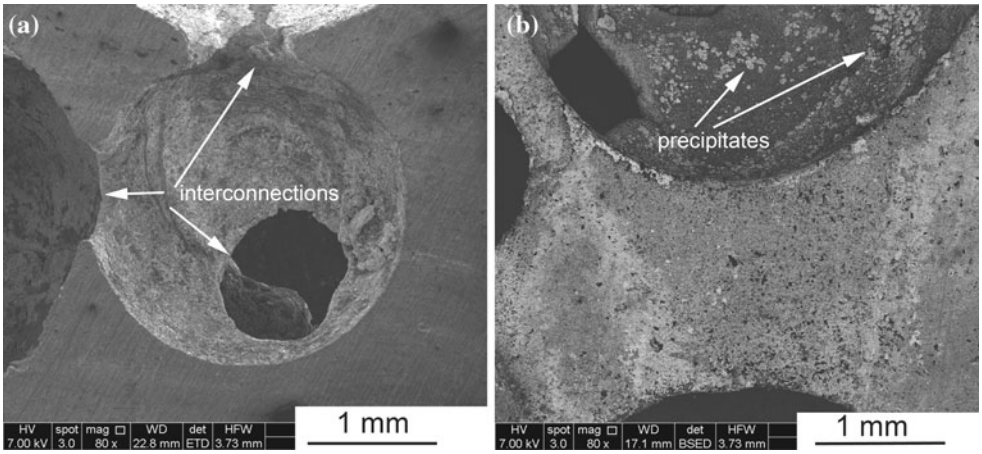

Fig. 8 SEM images of a 60 % porous lead foam showing **a** interconnections of a pore, and **b** precipitates on the foam sample surface and interior of the cells

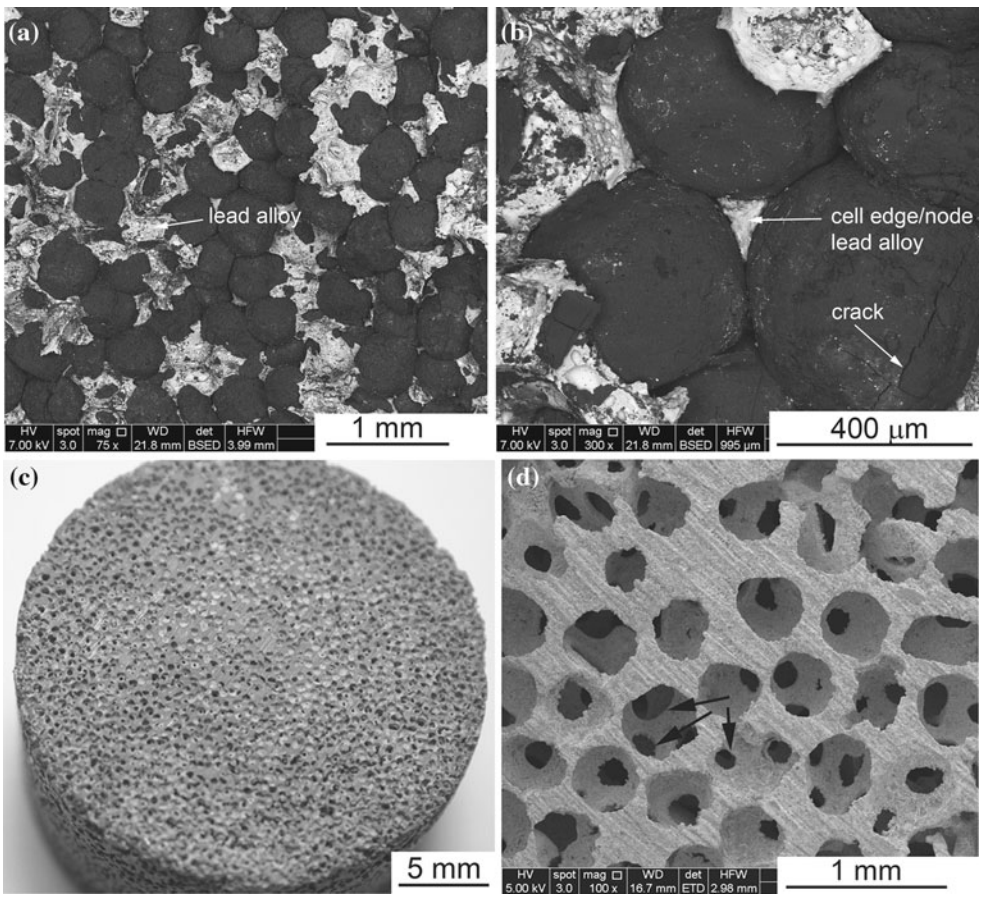

Fig. 9 SEM images of a 74 % porous lead foam **a** and **b** before salt particles removed; lead alloy is seen *white* and salt particles *black*, and **c** and **d** after salt particles removed; arrows show the interconnections with neighboring cells

Lead alloy foams prepared using salt particles as space holder had porosities of 65 and 74 %. It should be noted that the maximum porosities which can be achieved using space holders are limited to the values below 80 % [9]. Figure 9a, b show SEM images of a foam sample before, and Fig. 9c, d after dissolution of space holder. In these pictures, cast lead alloy are seen white, and salt particles are seen black. The liquid lead alloy is infiltrated efficiently through cell edges and nodes as seen in Fig. 9b. The foam cell sizes seen in Fig. 9c are also relatively homogeneous. Similar to the foams prepared using silica beads, foams prepared using salt particles have open cell structure: the cells have few interconnections with neighboring cells as shown with arrows in Fig. 9d. The size of the interconnections is measured to be approximately 100 μm.

Typical compression stress–strain curves of lead foams prepared by casting route represent characteristics of elastic–plastic foam deformation behavior as shown in Fig. 10. The stress–strain curve composes of three distinct regions (shown by the numbers in Fig. 10): (1) the linear elastic, (2) plateau, and (3) densification regions. The collapse stress (σ_c) is calculated by proportional limit (inset of Fig. 10). The foam elastic modulus (E) is calculated as the slope of the initial elastic region. The densification strain (ε_d) is calculated as the intersection of the tangent to the stress plateau regime and densification regime [17]. The compression stress–strain curves of lead alloy foams prepared using silica beads and salt particles are shown together in Fig. 11. In the same figure, the compression stress–strain curve of bulk lead alloy is also shown for comparison. It is clearly seen in the same figure, as the porosity increases, collapse stress, plateau stress, and elastic modulus decrease.

Figure 12 shows the variations of the elastic modulus, collapse stress, and densification strain of lead alloy foam with relative density. The collapse stress and elastic modulus data are further fitted with the following scaling relation [18]:

$$X_f = X_b C(\rho^*)^y \quad (2)$$

where X_f is the collapse stress or elastic modulus of foam, X_b is the yield strength or elastic modulus of bulk alloy, C is a constant, y is the exponential constant and ρ^* is the relative density, which is defined as

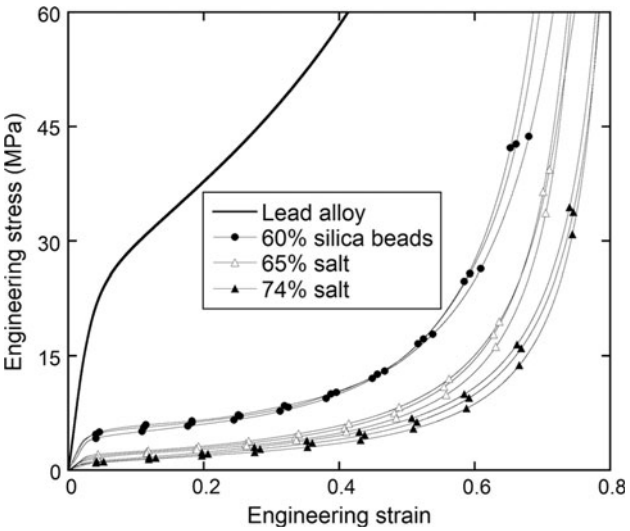

Fig. 11 Compression stress–strain curves of lead alloy foams prepared by casting route and bulk lead alloy, showing the effect of porosity on the plateau stress and elastic modulus

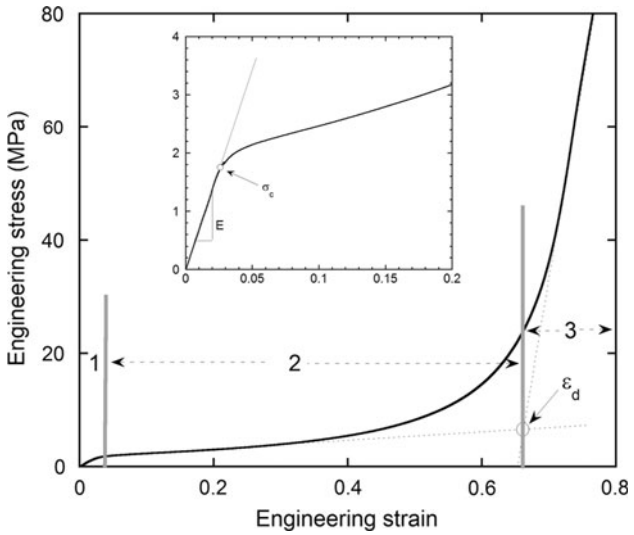

Fig. 10 Typical compression stress–strain curve of lead foams prepared by casting route showing characteristic three distinct deformation regions: linear elastic, plateau, and densification

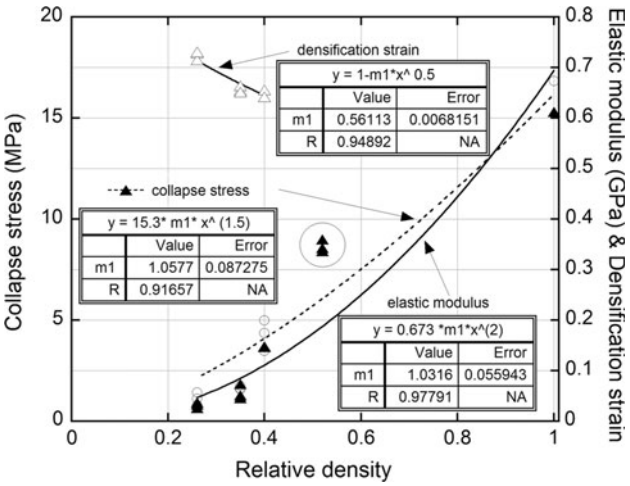

Fig. 12 The variation of collapse stress, elastic modulus, and densification strain of prepared lead foams as function of relative density and fitting results with Eqs. 2 and 4

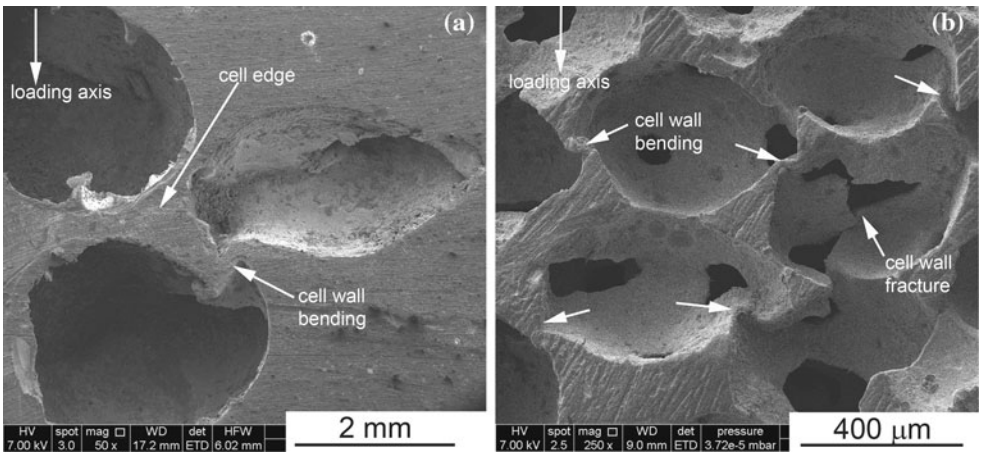

Fig. 13 SEM images of **a** a foam sample prepared using silica beads and deformed until about 0.3 strains, and **b** a foam sample prepared using salt particles and deformed until about 0.21 strain

$$\rho^* = \left(\frac{\rho_f}{\rho_b}\right) \tag{3}$$

where ρ_f and ρ_b are the densities of foam and foam cell wall alloy, respectively. The values of y for collapse stress and elastic modulus of open cell foams were reported to be 1.5 and 2, respectively [18]. The yield strength and elastic modulus of lead alloy used were determined experimentally, and found sequentially as 15.3 MPa and 0.673 GPa, respectively. The collapse stresses of the foams prepared by powder metallurgy with 48 % porosity are shown in Fig. 12 by a circle. The fitting parameter of C for collapse stress and elastic modulus of the prepared foams are found to be nearly 1 as shown in Fig. 12. The value of C for the elastic modulus of open cell foams was previously shown to be nearly 1 [18], matching the predicted value of C for the prepared lead alloy foams, while the value of C predicted for collapse stress is higher than the reported C value, 0.3 [18]. The imperfections such as curved, wrinkled and missing cell walls, voids on the cell edges and cell walls, and non-uniform density may lead to discrepancy between experimental and theoretical collapse stress values. The densification strain of open cell foams is described with the following scaling relation [19]:

$$\varepsilon_d = 1 - \alpha_o(\rho^*)^{1/2} \tag{4}$$

where α_o is a constant for particular foam structure. The fitting densification strains of the studied foams give a value of 0.56 for α_o (Fig. 12). Depending on the cell wall topology, the value of α_o was reported to vary between 0.7 and 1.55 for open cell foams. The variations between the methods of determination of densification strain may lead to differences between the predicted values of α_o. The densification strains of commercial metallic foams ranged between 0.4 and 0.9 [20], and the densification strains of the prepared foams were within this range.

Foam samples prepared using silica beads, and salt particles deformed until about 0.3 and 0.21 strain were cut through cross-section, and prepared metallographically to investigate the cell wall and edge deformation. The SEM image of a foam sample prepared using silica beads shown in Fig. 13a indicates that the deformation in the collapse region proceeds with cell edge crushing over the cell walls, showing typical deformation behavior of elastic–plastic open cell foam deformation. It is also observed that the collapse starts initially at the interconnection regions, and thin cell walls are observed to occasionally rupture. A similar foam deformation mechanism is also found in foam samples prepared using salt particles (Fig. 13b). The deformation proceeds with cell wall bending and tearing as marked with arrows in Fig. 13b.

Conclusions

Open cell lead foams with 48, 60, 65, and 74 % porosity were prepared through powder metallurgical and casting routes using ammonium bicarbonate, silica beads, and salt particles as space holder. The resulting foam samples resembled open cell foam structure: each cell had interconnections with neighboring cells. Small-sized lead (II) fluoride precipitates were observed in the interior of cells in the foam samples prepared using silica beads, mainly resulting from the reaction between silica beads and HF acid in the space holder removal stage. The compression stress–strain curves of foam samples prepared by powder metallurgical route using ammonium bicarbonate space holder showed brittle deformation following the initial elastic deformation region, while the foam samples prepared by casting route using silica beads and salt particles showed typical ductile metal foam deformation behavior, involving cell wall crushing and tearing. For designing

battery electrodes with lead foams, the collapse stresses, densification strains, and elastic moduli of the prepared foams were further fitted with the scaling relations. The discrepancy between experimental and theoretical scaling parameters was finally attributed to the imperfections such as curved, wrinkled, and missing cell walls, voids on the cell edges and cell walls, and non-uniform foam density.

References

1. Linden D, Reddy T (2001) Handbook of batteries, 3rd edn. McGraw-Hill Professional, New York
2. Gyenge E, Jung J, Mahato B (2003) J Power Sources 113(2):388–395. doi:10.1016/s0378-7753(02)00553-0
3. Irretier A, Banhart J (2005) Acta Mater 53(18):4903–4917. doi:10.1016/j.actamat.2005.07.007
4. Tabaatabaai SM, Rahmanifar MS, Mousavi SA, Shekofteh S, Khonsari J, Oweisi A, Hejabi M, Tabrizi H, Shirzadi S, Cheraghi B (2006) J Power Sources 158(2):879–884. doi:10.1016/j.jpowsour.2005.11.017
5. Gyenge E, Jung J, Splinter S, Snaper A (2002) J Appl Electrochem 32(3):287–295
6. Dai CS, Zhang B, Wang DL, Yi TF, Hu XG (2006) Mater Chem Phys 99(2–3):431–436. doi:10.1016/j.matchemphys.2005.11.014
7. Belhadj A-E, Kaoua S-A, Azzaz M, Bartout JD, Bienvenu Y (2008) Mater Sci Eng A 494(1–2):425–428. doi:10.1016/j.msea.2008.04.040
8. Bertolino G, Gruttadauria A, Arneodo Larochette P, Castrodeza EM, Baruj A, Troiani HE (2011) Intermetallics 19(4):577–585. doi:10.1016/j.intermet.2010.12.008
9. Banhart J (2001) Prog Mater Sci 46(6):559–632
10. Dizlek ME, Guden M, Turkan U, Tasdemirci A (2009) J Mater Sci 44(6):1512–1519. doi:10.1007/s10853-008-3038-7
11. Wang QZ, Cui CX, Liu SJ, Zhao LC (2010) Mater Sci Eng A Struct Mater Prop Microstruct Process 527(4–5):1275–1278. doi:10.1016/j.msea.2009.10.062
12. Wen CE, Mabuchi M, Yamada Y, Shimojima K, Chino Y, Asahina T (2001) Scripta Mater 45(10):1147–1153. doi:10.1016/s1359-6462(01)01132-0
13. Machavaram VR, Badcock RA, Fernando GF (2007) Sens Actuators A 138(1):248–260. doi:10.1016/j.sna.2007.04.007
14. Patnaik P (2003) Handbook of inorganic chemicals. McGraw-Hill, New York
15. Yamada Y, Shimojima K, Sakaguchi Y, Mabuchi M, Nakamura M, Asahina T, Mukai T, Kanahashi H, Higashi K (1999) J Mater Sci Lett 18(18):1477–1480
16. Beck F, Krohn H (1984) J Power Sources 12(1):9–30. doi:10.1016/0378-7753(84)80010-5
17. Paul A, Ramamurty U (2000) Mater Sci Eng A 281(1–2):1–7. doi:10.1016/s0921-5093(99)00750-9
18. Ashby M, Medalist R (1983) Metall Mater Transac A 14(9):1755–1769. doi:10.1007/bf02645546
19. Chan KC, Xie LS (2003) Scripta Mater 48(8):1147–1152
20. Ashby MF, Evans AG, Fleck NA, Gibson LJ, Hutchinson JW, Wadley HNG (2000) Metal foams: a design guide. Butterworth-Heinemann, Boston